Environment. Technology. Resources. Rezekne, Latvia
Proceedings of the 14th International Scientific and Practical Conference. Volume 3, 262-270

A Thermal Model for Wire Arc Additive Manufacturing

Manahil Tongov
Department of Material Sscience and Technology
Technical University of Sofia
Sofia, Bulgaria
Center of Welding
IMSETCHA "Acad. A. Balevski" Bulgarian Academy of Sciences
Sofia, Bulgaria
tongov@tu-sofia.bg

Vladimir Petkov
Institute of Metal Science, Equipment and Technologies with with Center for Hydro- and Aerodynamics (IMSETCHA)
"Acad. A. Balevski" Bulgarian Academy of Sciences
Sofia, Bulgaria
vladimir2pe@yahoo.com

***Abstract*. Layer-by-layer detailing processes, which used wire and electric arc - wire arc additive manufacturing (WAAM), are among the most productive in 3D metal printing technologies. From this point of view, the solution of the thermal task, and subsequently of the deformation problem, are particularly relevant. It is natural that these simulation modelling processes are closely related to welding, but at the same time it is necessary to take into account particularities that are crucial for WAAM and are not always relevant in welding. In this research, one such model is proposed, which takes into account the gradual filling of the working space with the deposited metal. The specific issues related to the construction of the model, the definition of the heat source and the first layer formation in the conditions of WAAM are considered. The obtained numerical results enable the prediction of the layer dimensions.**

Keywords: modelling; wire arc additive manufacturing.

I. INTRODUCTION

The processes of wire and arc additive manufacturing (WAAM) are close to the corresponding welding processes. This closeness is expressed both in their realization and in their research. Simulation processes are no exception in this regard. The main directions in the study of processes and the solution of specific technological tasks through the methods of simulation modelling can be presented in several groups: solving the heat problem in the parts manufactured by WAAM [1]÷[10]; solving a heat and fluid tasks with modelling the formation of the layer [11]÷[18]; determining the geometry of the layers using the technological parameters [19]÷[25]; optimal design of the rooting [1], [9], [10], [23] and [27]. When modelling heat processes, the Goldak heat source [1÷5] is most often used. It replaces the action of the welding arc with a volumetric heat source in the metal with a density of the released power $q[W/m^3]$. Equation (1) shows the definition of the base variant in a moving coordinate system related to the heat source. The effective heat output of the arc is $q_{eff} = \eta UI$. The density distribution function of the heat generated amount is illustrated in Fig.1. In addition to the efficiency factor η this heat source has 4 geometric parameters a_f, a_r, b and c (Fig.2), which can be used for its calibration.

$$q = \begin{cases} q_{eff}\dfrac{6\sqrt{3}f_f}{\pi\sqrt{\pi}a_f bc}\exp\left(-3\left(\dfrac{x^2}{a_f^2}+\dfrac{y^2}{b^2}+\dfrac{z^2}{c^2}\right)\right) & x \le 0 \\ q_{eff}\dfrac{6\sqrt{3}f_r}{\pi\sqrt{\pi}a_r bc}\exp\left(-3\left(\dfrac{x^2}{a_r^2}+\dfrac{y^2}{b^2}+\dfrac{z^2}{c^2}\right)\right) & x \ge 0 \end{cases} \quad (1)$$

The coefficients f_f and f_r determine the energy distribution between the two ellipsoids. In order to have continuity of the function from equation (1) it is necessary to respect the ratio $f_f/a_f = f_r/a_r$. The sum of these two coefficients is equal to two, which is related to the normalization of the function, and they can be determined by equations (2). This heat source is convenient when there is a significant penetration and the presence of a keyhole. Varieties aimed at solving specific problems are also used - one such example is given in [2]. In the processes under consideration, the formation of a deep keyhole can be prevented, and is often undesirable.

$$f_f = \frac{2a_f}{a_f + a_r} \qquad f_r = \frac{2a_r}{a_f + a_r} \quad (2)$$

Print ISSN 1691-5402
Online ISSN 2256-070X
https://doi.org/10.17770/etr2023vol3.7212

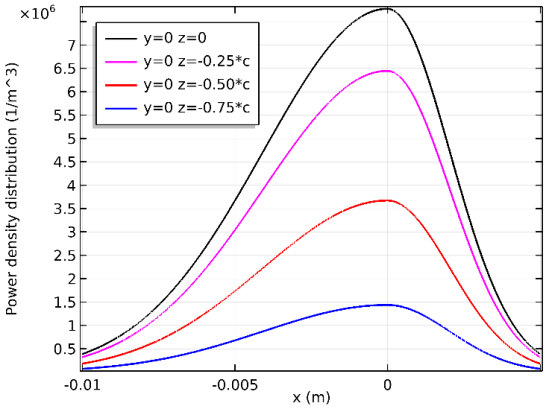

Fig. 1. Power density distribution for Goldak heat source with parameters (in mm) $a_f = 10$, $a_r = 5$, $b = 8$ and $c = 4$.

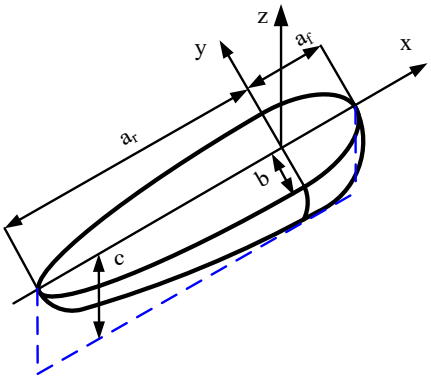

Fig. 2. Geometric interpretation of Goldak heat source.

Gaussian normally distributed heat source is also used often [6÷9, 24, 25]. It can have a different distribution along z axis (Fig. 3). The general form can be represented by equation (3). Here k is the heat source concentration coefficient (1/m^2); k/π is a normalizing factor for the two-dimensional normal distribution and the heat flux density along the arc axis in the plane of interaction of the welding arc with the metal is equal to $q_{eff}k/\pi$; $f(z)$ is an attenuation function of the released heat (1/m), which is normalized according to (4) or (5) where h_{pr} is the penetration depth.

$$q = q_{eff}\frac{k}{\pi}\exp\left(-kr^2\right)f(z) \tag{3}$$

$$r^2 = x^2 + y^2$$

$$\int_{-\infty}^{0} f(z)dz = 1 \tag{4}$$

$$\int_{0}^{h_{pr}} f(z)dz = 1 \tag{5}$$

When solving only a heat problem, the shape of the weld pool is determined by the forces acting on it. Equation (6) [2] is used to determine the weld pool free surface shape. The heat flux is transmitted through the surface of the weld pool.

$$\sigma\left[\frac{\left(1+\varphi_y^2\right)\varphi_{xx} - 2\varphi_x\varphi_y\varphi_{xy} + \left(1+\varphi_x^2\right)\varphi_{yy}}{\left(1+\varphi_x^2+\varphi_y^2\right)^{3/2}}\right] = \tag{6}$$
$$= \rho g\varphi + P - \lambda$$

where σ is the surface tension (N/m); φ – the displacement of the surface (mm); g – ground acceleration (m/s2); P – arc pressure (N/mm2); λ – Lagrange multiplier

When solving fluid and temperature problems to describe the movement of the liquid phase and the formation of the free surface of the weld pool, in addition to the heat balance equation, the fluid continuity equation and the Navier-Stokes equation, describing the movement of a viscous liquid, are solved. To describe this movement, the following factors are considered [12, 28]: the surface tensions force (equation 7); the gravitational force taking into account the change of density depending on the temperature combined with electrodynamic force (equations 8÷11); pressure of welding arc – a model (equations 12÷14) similar to the Koldak heat source model is used [12, 29]

$$P_\sigma = \sigma\kappa \qquad \sigma = \sigma_L + \alpha_\sigma\left(T - T_L\right) \tag{7}$$

$$\mathbf{F_b} = \left(\mathbf{j}\times\mathbf{B}\right) - \rho\mathbf{g}\beta\Delta T \tag{8}$$

$$P_{ex} = -\frac{\mu_m I^2}{4\pi^2 j^2 r}\exp\left(-\frac{r^2}{2j^2}\right)\times$$
$$\times\left[1+\exp\left(-\frac{r^2}{2j^2}\right)\right]\left(1-\frac{z}{L_0}\right)^2\frac{x}{r} \tag{9}$$

$$P_{ey} = -\frac{\mu_m I^2}{4\pi^2 j^2 r}\exp\left(-\frac{r^2}{2j^2}\right)\times$$
$$\times\left[1+\exp\left(-\frac{r^2}{2j^2}\right)\right]\left(1-\frac{z}{L_0}\right)^2\frac{y}{r} \tag{10}$$

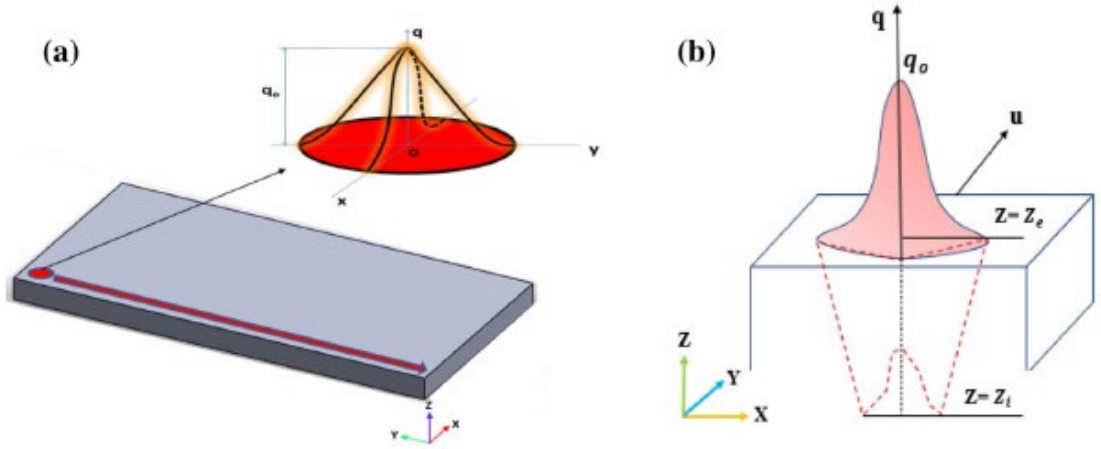

Fig. 3. Two variants of a Gaussian heat source – surface (a) and volumetric with a conical depth distribution (b) [2].

$$P_{ez} = -\frac{\mu_m I^2}{4\pi^2 j^2 r}\exp\left(-\frac{r^2}{2j^2}\right)\times \times\left(1-\frac{z}{L_0}\right)-\rho g\beta\Delta T \tag{11}$$

$$p_{arc}(x,y) = K_p\frac{3\mu_m I^2}{2\pi^2\left(a_{pf}\mid a_{pr}\right)}\times \times\exp\left(-3\left(\frac{(x-vt)^2}{a^2}+\frac{y^2}{b_p^2}\right)\right) \tag{12}$$

$$a=\begin{cases} a_{pf} & x\geq vt \\ a_{pr} & x<vt \end{cases} \tag{13}$$

$$\iint_{\Omega} p_{arc}(x,y)dS-\frac{\mu_m I^2}{4\pi}=0 \tag{14}$$

In [19], it was proposed that the shape of the cross section of a single welded layer (Fig. 4) be described by a second degree equation (15). After expressing the crossectional area of the layer by the feed rate v_e, the diameter of the electrode wire d_e and the travel speed v_w, a relationship was obtained connecting these parameters to the shape of the layer (equation 16). Experiments were then conducted with hybrid laser MIG/MAG surfacing and a regression equation was derived, enabling the height of the layer to be determined depending on the travel speed and the wire feed rate (Equation 17). The wire feed rate is changed from 4.7 to 10.4 m/min, and the travel speed is in the range of 0.6 to 1.1 m/min.

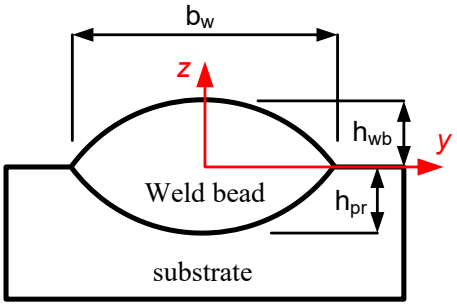

Fig. 4. Weld bead dimensions.

$$y = h_{wb}\left[1-\left(\frac{2z}{b_w}\right)^2\right] \tag{15}$$

$$y = h_{wb}\left[1-\left(\frac{16h_{wb}v_w}{3\pi v_f d_e^2}z\right)^2\right] \tag{16}$$

$$h_{wb} = 3.0299-4.9778v_w+0.18497v_e- -0.13833v_w v_e+2.5610v_w^2+0.0029945v_e^2 \tag{17}$$

The described parabolic model of the weld bead shape was used in the MIG/MAG process [20]. The profile shape of the bead can also be described using equations (18) or (19). These two models and the parabolic model are compared in [21]. The width and height of the beads were measured, as well as the cross-sectional area. The areas were calculated using the three models and it was shown that the parabolic model gives results closer to the measured ones. The parabolic model has also been used to describe the layer geometry in multipass welding [19, 22].

$$y = h_{wb} \cos\left(\frac{\pi z}{b_w}\right) \quad (18)$$

$$y = \sqrt{R^2 - z^2} + h_{wb} - R \quad (19)$$

II. MATERIALS AND METHODS

As part of this study, experiments were conducted to determine the shape of the layers. Conventional GMAW equipment was used. The filler material is SG2 with a diameter of 0.8 mm and its chemical composition according to the manufacturer's certificate is shown in Table I. WAAM starts on a 4x150x350 mm plate from S355 steel and a vertical wall is built. The parameters of the process are: welding current – 76 A; arc voltage – 17 V; feed rate – 4.6 m/min; welding speed – 12 cm/min; shielding gas Ar+18%CO_2. The experimental setup used is shown in Fig. 5. To determine the shape of the applied layers, a cross-section of the layers was prepared for metallographic investigation (Fig. 6). The surface of the section was machined according to standard metallographic profile preparation procedure by grinding and polishing and was etched with 5% HNO_3.

TABLE I. CHEMICAL COMPOSITION OF THE USED WELDING WIRE (BALANCED – FE), MASS. %

C	***Mn***	***Si***	***P***	***S***
0.07	1.45	0.82	0.005	0.10
Ni	Cr	V	Cu	
0.02	0.03	0.004	0.03	

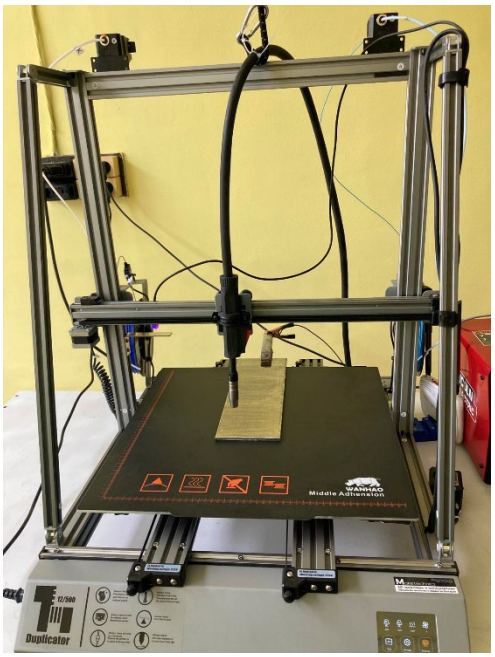

Fig. 5. Experimental set-up.

In process modelling, a heat task is solved using FEM. The used thermal properties of the metal are shown in Fig.7÷Fig.9.

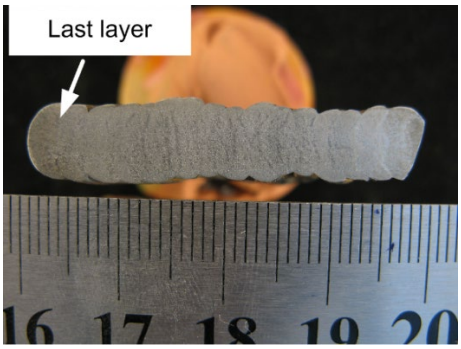

Fig. 6. Cross-section profile.

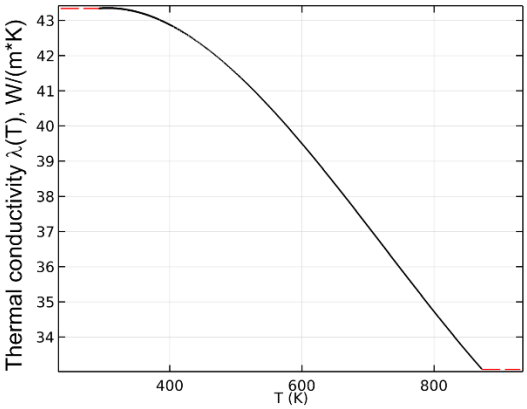

Fig. 7. Thermal conductivity of used metal.

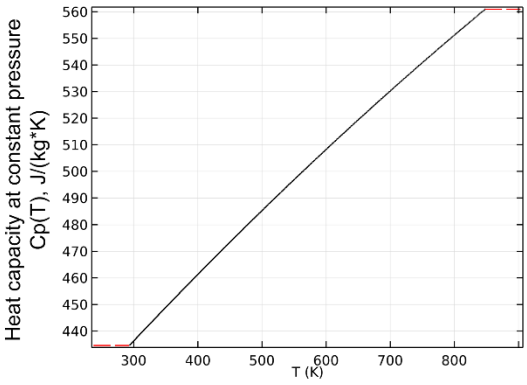

Fig. 8. Heat capacity at constant preasure for used metal.

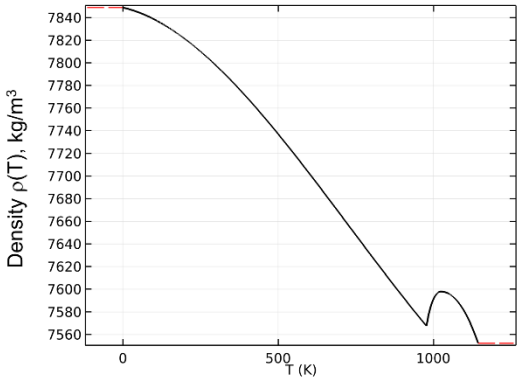

Fig. 9. Density of used metsl.

III. RESULTS AND DISCUTIONS

The properties of the layer material are obtained by combining those of the metal and those of the air. A transition zone is defined in front of the welding arc (Fig. 10). In this transition zone, a transition function $\varphi(x)$ is defined in the movable coordinate system associated with the welding arc (Fig. 11). The layer material properties in the moving coordinate system are defined as

$$\rho_w = \varphi(x)\rho_{air} + [1-\varphi(x)]\rho_{steel} \quad (20)$$

$$\lambda_w = \varphi(x)\lambda_{air} + [1-\varphi(x)]\lambda_{steel} \quad (21)$$

$$Cp_w = \varphi(x)Cp_{air} + [1-\varphi(x)]Cp_{steel} \quad (22)$$

The change in the properties of the environment is illustrated in Fig.12 and Fig. 13.

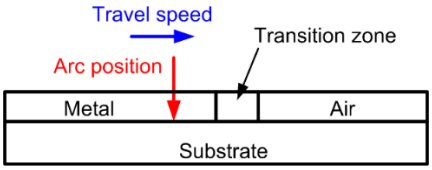

Fig. 10. Transition zone in layer material.

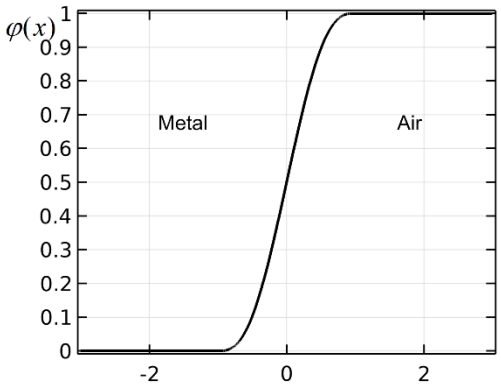

Fig. 11. Transition function.

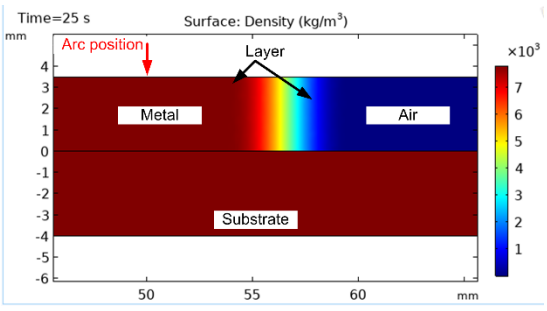

Fig. 12. Realization of transition function.

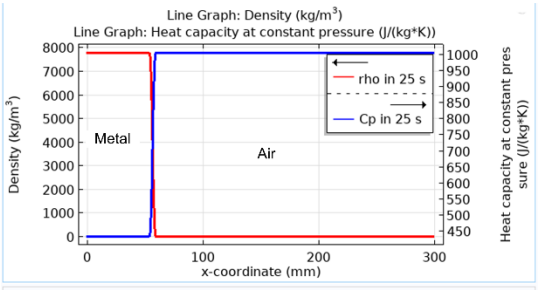

Fig. 13. Changing the properties of the medium in front of the welding arc.

The cross-sectional shape of the first layer (Fig. 14) can be represented as a segment of an ellipse with dimensions shown in Fig. 15. The area of this cross-section is defined as $A_{w1} = ab\arccos(z_0/b) - y_0 z_0$ and is actually determined by the wire feed rate V_{wf}, the welding speed V_w, and the electrode wire diameter d_e as $A_{w1} = 0.25\pi d_e^2 V_{wf}/V_w$. This area can be expressed in terms of the dimensions of the ellipse:

$$A_{w1} = \frac{b_w h_w}{2(1-\beta)}\left[\frac{\arccos(\beta)}{\sqrt{1-\beta^2}} - \beta\right] \quad (23)$$

where $\beta = \dfrac{z_0}{z_0 + h_w} \rightarrow 0 \le \beta < 1$.

To show that this way of representing the geometry of the first layer gives good results, we will use the experimental data from [21]. There, three different ways of representing the layer geometry are compared and it is shown that the best results are obtained when using a parabolic dependence. Using these data, the value of β was determined as varied in the permissible interval through 0.1, which is a rather rough determination of this quantity. Nevertheless, the accuracy with which the section of the layer is calculated is higher than that calculated by means of a parabolic section (Table 2). In this table A_p is the area of parabolic section, $\varepsilon(A_p)$ and $\varepsilon(A_{w1})$ are the absolute values of errors in determining A_p and A_{w1}, respectively. The mean values of these errors are $\varepsilon_{ave}(A_p) = 5.98\%$ and $\varepsilon_{ave}(A_{w1}) = 2.009\%$.

To predict the dimensions of the welded bead, the heat problem is solved. When solving it, the reaching of the solidus temperature along the transition line between the substrate and the applied layer is considered as a condition (Fig. 16). At the same time, in the middle of the layer (Fig. 17), a temperature not lower than the temperature of the liquidus must be reached. The height of the layer h_w and the parameter β, are varied, and the width of the layer is determined by the equation

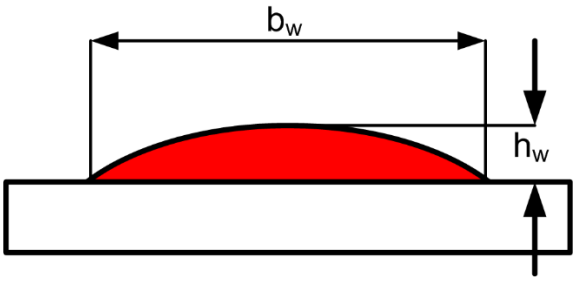

Fig. 14. Eleptical cross-sectional shape of the first layer.

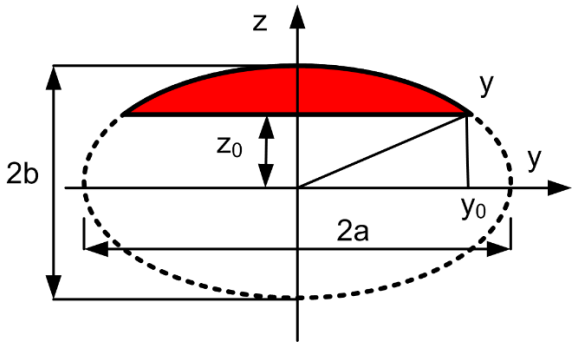

Fig. 15. Dimensions of ellipse.

TABLE II. EXPERIMENTAL DATA FOR BEAD DIMENSIONS FROM [21] AND CALCULATED PARAMETERS OF ELLIPTICAL SEGMENT

b_w	h_w	A measured	A_p	$\varepsilon(A_p)$	β	z_0	a	b	A_{w1}	$\varepsilon(A_{w1})$
mm		mm^2		%		mm			mm^2	%
6.488	3.047	15.08	13.178	12.61	0.1	0.34	3.26	3.39	15.13	0.36
6.128	2.683	11.729	10.962	6.53	0.5	2.68	3.54	5.37	11.66	0.59
7.387	2.319	10.556	11.422	8.20	0.9999	23187	261.18	23190	11.42	8.19
4.994	2.426	8.445	8.078	4.34	0.6	3.64	3.12	6.07	8.47	0.27
8.95	2.876	18.096	17.158	5.18	0.6	4.31	5.59	7.19	17.99	0.59
7.193	2.448	10.858	11.738	8.10	0.9999	24477	254.32	24480	11.74	8.11
5.174	2.533	9.048	8.738	3.42	0.7	5.91	3.62	8.44	9.04	0.11
8.798	3.346	21.543	19.628	8.88	0.3	1.43	4.61	4.78	21.60	0.26
7.899	2.961	16.756	15.594	6.93	0.4	1.97	4.31	4.94	16.86	0.60
7.249	2.662	12.567	12.863	2.35	0.9999	26617	256.30	26620	12.86	2.37
7.193	2.533	11.6	12.149	4.73	0.9999	25327	254.32	25330	12.15	4.71
11.759	3.796	33.176	29.754	10.31	0.2	0.95	6.00	4.75	33.41	0.71
8.079	2.94	16.588	15.833	4.55	0.6	4.41	5.05	7.35	16.60	0.07
7.788	2.811	13.27	14.596	9.99	0.9999	28107	275.35	28110	14.59	9.98
7.539	2.341	11.059	11.765	6.38	0.9999	23407	266.55	23410	11.77	6.39
8.51	2.24	13.007	12.708	2.29	0.8	8.96	7.09	11.20	12.99	0.16
10.721	3.346	26.139	23.719	9.25	0.3	1.43	5.62	4.78	26.32	0.70
10.002	3.218	21.782	21.456	1.49	0.9	28.96	11.47	32.18	21.68	0.46
9.116	3.047	19.604	18.517	5.54	0.5	3.05	5.26	6.09	19.70	0.48
8.286	2.747	15.683	15.176	3.23	0.7	6.41	5.80	9.16	15.70	0.09
11.233	3.304	25.133	24.739	1.56	0.9	29.74	12.89	33.04	25.00	0.52
9.905	3.282	22.62	21.672	4.19	0.6	4.92	6.19	8.21	22.72	0.44
7.332	2.854	15.08	13.951	7.48	0.4	1.90	4.00	4.76	15.08	0.01

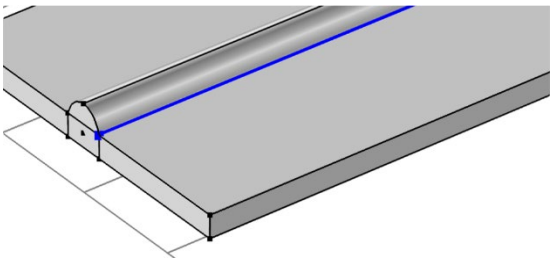

Fig. 16. On this line solidus temperature must be reached.

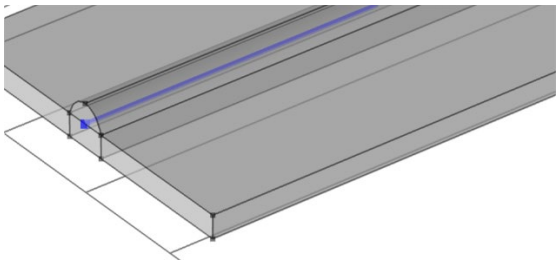

Fig. 17. The temperature reached on this line must be no lower than the liquidus temperature.

$$b_w = \frac{2(1-\beta)A_{w1}}{h_w}\left[\frac{\arccos(\beta)}{\sqrt{1-\beta^2}} - \beta\right]^{-1} \qquad (24)$$

The axisymmetric Gaussian heat source is considered as acting on the surface of the layer and substrate. It is defined in a movable coordinate system related to the movement of the welding arc. The heat flow through the plane containing the y_1 axis and perpendicular to the axis of the welding arc (Fig. 18) is described by the equation

$$f(x, y_1) = q_{eff}\frac{k}{\pi}\exp\left(-k\left(x^2 + y^2\right)\right) \qquad (25)$$

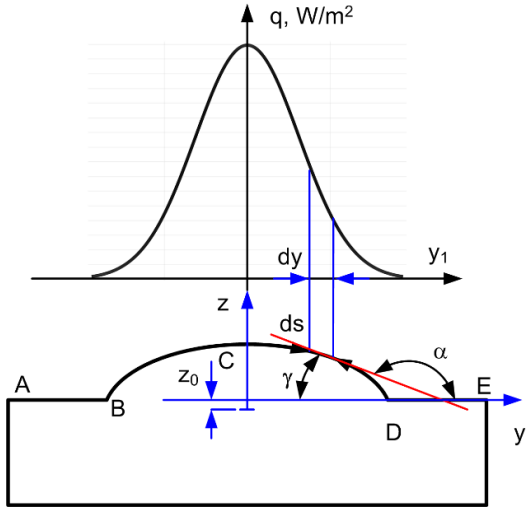

Fig. 18. Heat source.

The concentration coefficient of the heat source is related to the standard deviation and $k = 1/(2\sigma^2)$. The effective radius of the heating spot is $r_{arc} = 3\sigma$ (virtually all the heat power is transmitted through the heating spot). In this way, the concentration factor of the heat source can be determined by the effective radius of the heating spot $k = (9/2)r_{arc}^2$. Substituting this value in (25) we get the heat flow distribution function

$$q(x, y_1) = q_{eff} \frac{9}{2\pi r_{arc}^2} \exp\left(-\frac{9}{2r_{arc}^2}\left(x^2 + y^2\right)\right) \quad (26)$$

When applying the first layer, the heat flow is transmitted to both the applied layer and the substrate. Equation (26) is used to describe the interaction of the electric arc with the substrate (sections AB and DE in Fig. 18). We determine the density of the heat flow through the surface of the applied bead as follows. In the direction of the x axis, there is no change in the way of calculation. In the direction of the y axis, we consider a section with a width of dy. The heat flow that passes through this section is distributed over a section of the surface of the applied layer with length ds. This means that in this case the dependency $q(x, y) = q(x, y_1)\cos(\gamma)$ should be used. The curve describing the cross-section of the layer $z(y)$ (in this case an ellipse) is defined in the Oyz coordinate system. From Fig.18 it can be seen that $tg(\gamma) = -tg(\alpha)$ and $\cos(\gamma) = -\cos(\alpha)$ can be determined by the derivative of the function $z(y)$. Equation (27) gives the final result, which is also illustrated in Fig.19

$$\cos(\gamma) = \sqrt{\frac{1 - \left(\frac{y}{a}\right)^2}{1 - \left(\frac{y}{a}\right)^2\left[1 - \left(\frac{b}{a}\right)^2\right]}} \quad (27)$$

Thus, the final model of the heat source is

$$q(x, y) = \begin{cases} q_1(x, y) & for \quad AB \mid CD \\ q_1(x, y)\cos(\gamma) & for \quad BCD \end{cases} \quad (28)$$

where

$$q_1(x, y) = q_{eff} \frac{9}{2\pi r_{arc}^2} \exp\left(-\frac{9}{2r_{arc}^2}\left(x^2 + y^2\right)\right)$$

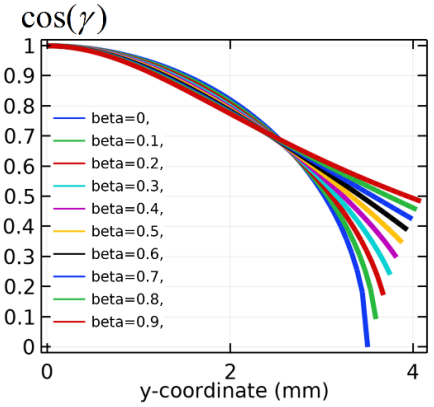

Fig. 19. Influence of the parameter β on cos(γ).

The results of the calculation of the temperature field are shown in Fig. 20 ÷ Fig. 25. Fig. 20 shows the temperature distribution along the upper surface of the substrate and the welded bead. It can be noted that the line delineating the width of the layer appears as a tangent to the isotherm of the solidus. This is also confirmed by Fig. 21, where the temperature distribution along the fusion line is shown. Also shown in the same figure are the temperature distributions along lines in the plane of the seam line, located at different distances from the top surface of the substrate. From these graphs, it can be concluded that the penetration depth along the seam line is slightly greater than 1 mm. Fig. 22 shows isotherms in the upper plane of the substrate. Here it can be seen that the solidus isotherm spans the entire width of the bead, i.e. there is good fusion between the substrate and the layer. In addition, here you can see the resulting width of the layer - 6 mm. The depth of the penetration along the seam line can be seen in Fig.23. This figure also shows the height of the layer. Fig. 24 and Fig. 25 show the isothermal surfaces and the general appearance of the temperature field, respectively. The resulting geometric dimensions of the layer match well with those shown in Fig. 6.

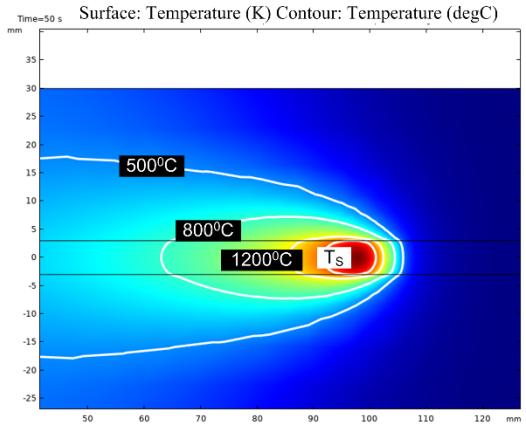

Fig. 20. Temperature distribution along the upper surface of the substrate and the welded bead.

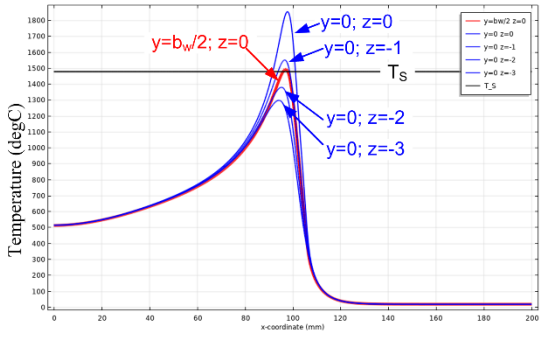

Fig. 21. Temperature distribution along the fusion line (red) and lines in the plane of the seam line at different depths in the substrate.

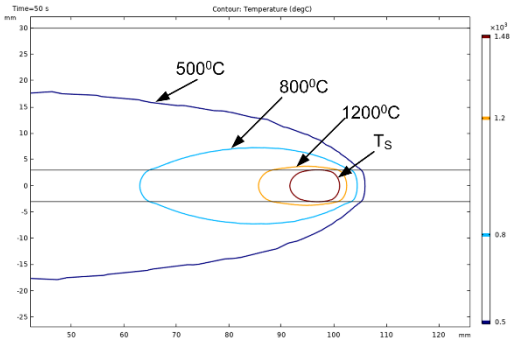

Fig. 22. Isotherms in the upper plane of the substrate.

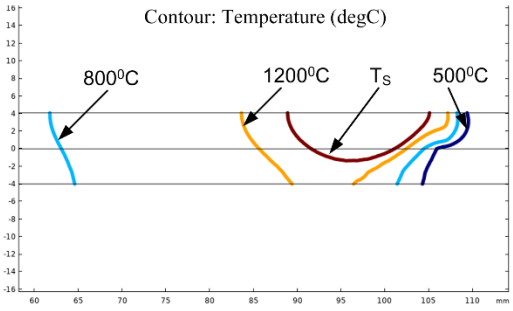

Fig. 23. The depth of the penetration along the seam line.

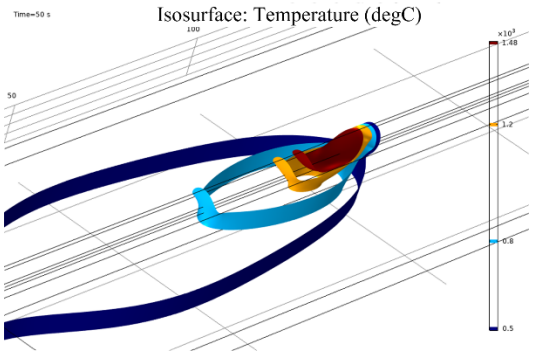

Fig. 24. Isothermal surfaces.

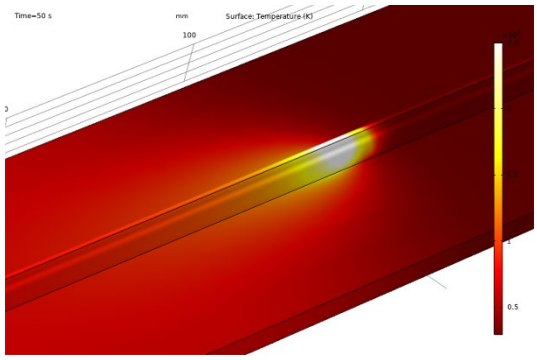

Fig. 25. General appearance of the temperature field.

IV. CONCLUTIONS

A methodology for simulation modeling of the thermal processes in the first layer during WAAM is proposed, which takes into account the current position of the welding torch and the completed length of the layer It has been shown that the representation of the layer cross-section by an elliptical segment gives a more accurate calculation of the cross-sectional area of the layer compared to the parabolic form. As a result of solving the heat problem, the width and height of the obtained layer were determined at set parameters of the regime (feed rate, travel speed, welding current, arc voltage). It is shown that along the fusion line the temperature reaches that of the solidus, and that fusion between the layer and the substrate is achieved. The proposed methodology can also be used in simulation modeling of multipass welding.

V. ACKNOWLEDGMENTS

The authors are grateful to the financial support of the Bulgarian National Science Fund, Contract No KP-06-H57/10, for carrying out the necessary research.

REFERENCES

[1] T. A. Rodrigues, V. Duarte, R.M. Miranda, T. G. Santos and J. P. Oliveira, "Current status and perspectives on wire and arc additive manufacturing (WAAM)", Materials vol.12, issure 7, art. ID 1121, 2019.

[2] K. Barath and M. Manikandan, "Assessment of process, parameters, residual stress mitigation, post treatments and finite element analysis simulations of wire arc additive manufacturing technique", Metals and Materials International, vol. 28, pp.54-111, 2022.

[3] V. Mishra, A. Babu, R Schreurs, U. Wu, M Hermans and C. Ayas, "Microstructure Estimation and Validation of ER110S-G steel structures produced by Wire and Arc Additive Manufacturing", Journal of Materials Research and Technology, vol. 23, pp. 3579-3601, 2023

[4] T. Zhang, H. Li, H. Gong, Y. Wu, X. Chen and X. Zhang, "Study on location-related thermal cycles and microstructure variation of additively manufactured inconel 718", Journal of Materials Research and Technology, vol. 18, pp. 3056-3072, 2022.

[5] J. Xiaolei, X. Jie, L. Zhaoheng, H. Shaojie, F. Yu and S. Zhi, "A new method to estimate heat source parameters in gas metal arc welding simulation process", Fusion Engineering and Design vol. 89, pp. 40– 48, 2014

[6] T. Mukherjee, W. Zhang and T. DebRoy, "An improved prediction of residual stresses and distortion in additive manufacturing", Computational Materials Science vol. 126 pp. 360–372, 2017

[7] H. Arora, R. Singh and G.S. Brar, "Thermal and structural modelling of arc welding processes: A literature review", Measurement and Control, vol 52 (7-8), pp. 955-969, 2019, SAGE Publications Sage UK: London, England

[8] N.P. Gokhale and P. Kala "Thermal analysis of TIG-WAAM based metal deposition process using finite element method" ,Materials Today: Proceedings, vol. 44, pp. 453-459, 2021.

[9] C. Xiaoxuan, S. Xin, Z. Zirong and S. Chen, "A Review of the Development Status of Wire Arc Additive Manufacturing Technology", Advances in Materials Science and Engineering Volume 2022, Article ID 5757484, 28 pages https://doi.org/10.1155/2022/5757484

[10] S. Pattanayak and S.K. Sahoo; "Gas metal arc welding based additive manufacturing - a review", CIRP Journal of Manufacturing Science and Technology, vol. 33, pp. 398-442, 2021.

[11] M. Chaturvedi, E. Scutelnicu, C.C. Rusu, L.R. Mistodie, D. Mihailescu and A.V. Subbiah; "Wire arc additive manufacturing: Review on recent findings and challenges in industrial applications and materials characterization", Metals, vol. 11, issure 6, art. ID 939, 2021.

[12] W.C. Ke, J.P. Oliveira, B.Q. Cong, S.S. Ao, Z.W. Qi, B. Peng and Z. Zeng,; "Multi-layer deposition mechanism in ultra high-frequency pulsed wire arc additive manufacturing (WAAM) of NiTi shape memory alloys", Additive Manufacturing, vol. 50, art. ID 102513, 2022

[13] X. Chen, C. Wang, J. Ding, P. Bridgeman and S. Williams, "A three-dimensional wire-feeding model for heat and metal transfer, fluid flow, and bead shape in wire plasma arc additive manufacturing",Journal of Manufacturing Processes, vol. 83, pp. 300-312, 2022.

[14] X. Zhou, H. Zhang, G. Wang and X. Bai, "Three-dimensional numerical simulation of arc and metal transport in arc welding based additive manufacturing", International Journal of Heat and Mass Transfer vol.103, pp. 521–537, 2016

[15] F. Hejripour, D. T. Valentine and D. K. Aidun, "Study of mass transport in cold wire deposition for Wire Arc Additive Manufacturing", International Journal of Heat and Mass Transfer vol. 125, pp. 471–484, 2018.

[16] X. Bai, P. Colegrove, J. Ding, X. Zhou, C. Diao, P. Bridgeman, J. Hönnige, H. Zhang and S. Williams, "Numerical analysis of heat transfer and fluid flow in multilayer deposition of PAW-based wire and arc additive manufacturing", International Journal of Heat and Mass Transfer vol. 124 pp. 504–516, 2018

[17] W. Ou et al. "Fusion zone geometries, cooling rates and solidification parameters during wire arc additive manufacturing", International Journal of Heat and Mass Transfer vol. 127, pp. 1084-1094, 2018

[18] W. Ou et al. "Determination of the control points for circle and triangle route in wire arc additive manufacturing (WAAM)", Journal of Manufacturing Processes vol. 53, pp. 84-98, 2020.

[19] S. Suryakumar, K.P. Karunakaran, Alain Bernard, U. Chandrasekhar, N. Raghavender and D. Sharma, "Weld bead modeling and process optimization in Hybrid Layered Manufacturing", Computer-Aided Design vol. 43, pp. 331–344, 2011

[20] L. Nguyen, J. Buhl, and M. Bambach. "Multi-bead overlapping models for tool path generation in wire-arc additive manufacturing processes." Procedia Manufacturing vol. 47, pp. 1123-1128, 2020

[21] J. Xiong, G. Zhang, H. Gao and L. Wu, "Modeling of bead section profile and overlapping beads with experimental validation for robotic GMAW-based rapid manufacturing", Robotics and Computer-Integrated Manufacturing vol. 29 issure 2, pp. 417-423, 2013

[22] D. Ding, Z. Pan, D. Cuiuri and H. Li, "A multi-bead overlapping model for robotic wire and arc additive manufacturing (WAAM)", Robotics and Computer-Integrated Manufacturing vol. 31, pp. 101-110, 2015

[23] B. Tomar, S, Shiva and T. Nath, "A review on wire arc additive manufacturing: Processing parameters, defects, quality improvement and recent advances", Materials Today Communications, vol. 31 art. ID 103739, 2022

[24] P. Shukla, B. Dash, D.V. Kiran and S Bukkapatnam, "Arc behavior in wire arc additive manufacturing process", Procedia Manufacturing, vol. 48, pp. 725-729, 2020.

[25] M. Benakis, D. Costanzo and A. Patran, "Current mode effects on weld bead geometry and heat affected zone in pulsed wire arc additive manufacturing of Ti-6-4 and Inconel 718", Journal of Manufacturing Processes vol. 60, pp. 61–74, 2020.

[26] V. A Hosseini et al. "Wire-arc additive manufacturing of a duplex stainless steel: thermal cycle analysis and microstructure characterization" Welding in the World vol. 63 pp. 975-987, 2019.

[27] R. Israr, J. Buhl, L. Elze and M. BamBach "Simulation of different path strategies for wire-arc additive manufacturing with Lagrangian finite element methods", LS-DYna Forum. 2018, Bamberg.

[28] C.S. Wu and L. Dorn, "Computer simulation of fluid dynamics and heat transfer in full-penetrated TIG weld pools with surface depression", Computational Materials Science vol 2q issure 2, pp. 341-349, 1994

[29] L. Nguyen, J. Buhl, R. Israr and M. Bambach, "Analysis and compensation of shrinkage and distortion in wire-arc additive manufacturing of thin-walled curved hollow sections", Additive Manufacturing vol. 47, art. ID 102365, 2021.

[30] X. Meng, G. Qin amd Z. Zou, "Sensitivity of driving forces on molten pool behavior and defect formation in high-speed gas tungsten arc welding", International Journal of Heat and Mass Transfer vol. 107, pp. 1119–1128, 2017.